Korean Journal of Chemical Engineering
https://doi.org/10.1007/s11814-024-00245-8

ORIGINAL ARTICLE

Characterization of the Ge@GeO_2-C Composite Anode Synthesized Using a Simple High-Energy Ball-Milling Process for Li-Ion Batteries

Hyun Woo Kim[1] · **Jinhyup Han**[2]

Received: 12 February 2024 / Revised: 2 July 2024 / Accepted: 28 July 2024

Abstract

To address the limitations of the current anodes of Li^+-ion batteries (LIBs), a Ge/GeO_2/carbon (Ge@GeO_2-C) composite was designed by introducing a high-energy ball-milling process for advanced LIBs. Ge@GeO_2-C is prepared and characterized by XPS, XRD, SEM, and TEM, which facilitate synthesis and provide controllability with respect to milling time. Interestingly, as the ball-milling time increased, the proportion of metallic Ge increased during the carbon thermal reduction reaction. The electrochemical characteristics of Ge@GeO_2-C are assessed using differential capacity analysis (dQ/dV) and galvanostatic charge–discharge techniques to confirm its viability as an anode material in LIBs. The results demonstrate decent initial and secondary capacities of approximately 1800 mAh g^{-1} (for the first cycle) and 838 mAh g^{-1} (for the second cycle) at a rate of C/60 by the reaction between Ge and the Li–Ge complex. Furthermore, post-mortem characterization was performed to gain an understanding of the material, suggesting future prospects for advanced LIBs.

Keywords Li^+ ion batteries · Ge anode · Alloy

Introduction

Lithium-ion batteries (LIBs) are primarily used in the electric vehicle (EV) and power storage industries [1–3]. Owing to the need for improved energy density and fast charging, research on anode materials other than graphite is essential. In particular, the energy density of LIB technology is currently at its limit. This problem is primarily due to the relatively low specific capacity of commercially available graphite-based negative electrodes (372 mAh g^{-1}) [4]. Owing to the rapidly increasing demand for LIBs, researchers have focused on high-performance anode materials [5–7].

As shown in Table 1, various materials, including metal oxides and group IV elements (such as Si, Ge, and Sn), have been considered as potential high-capacity anodes. In particular, Si- and Sn-based anode materials can store more than four moles of Li per mole of active material, which is a significant increase in capacity compared to graphite anodes. However, one of the biggest challenges with group IV elements is volume expansion, and numerous studies have been conducted to improve anode delamination from the copper foil after cycling [8].

The intrinsic issues and challenges of Si representing group IV elements are as follows:

1. Lithium (de)alloying can lead to a volume expansion ~ 420%, and its low electrical conductivity of 10^{-3} S/cm makes it challenging to commercialize [9].
2. The majority of expansion during lithiation occurs at the phase boundary between Li_xSi and Si. Mechanical fracture and pulverization are caused by repeated volume changes as stress generation differs with Si size and phase, which ultimately leads to loss of active material [10].
3. Si experiences unstable formation of the solid-electrolyte interphase (SEI) layer, and the SEI layer builds up continuously due to volume change during cycling [11].

Hyun Woo Kim and Jinhyup Han are co-first authors and contributed equally to this work. Corresponding Author: Prof. Jinhyup Han.

✉ Jinhyup Han
jhan@kmu.ac.kr

[1] Research Center for Materials Analysis, Korea Basic Science Institute (KBSI), Daejeon 34133, Republic of Korea

[2] Department of Chemical Engineering, Keimyung University, Daegu 42601, Republic of Korea

Published online: 01 August 2024

Table 1 Summary of group IV elements as anode materials for LIBs [23]

Element	Density (g cm^{-3})	Lithiated phase	Theoretical gravimetric capacity (mAh g^{-1})	Volume expansion
C	2.25	LiC_6	372	12%
Si	2.33	$Li_{4.4}Si$	4200	420%
Ge	5.32	$Li_{4.25}Ge$	1624	370%
Sn	7.26	$Li_{4.4}Sn$	994	260%
Pb	11.35	$Li_{4.4}Pb$	569	233%

In addition, there are several issues that impede the commercialization of Si anode representing Group 14. As the volume changes, the Si active material loses, resulting in a loss of electrical contact with its neighboring unit, conductive network and loss of electrical conductivity. And in terms of cycle retention, forming a stable and nice SEI layer is very helpful for long cycles, but the consumption of a significant amount of lithium due to continuous SEI formation ultimately blocks the electronic conduction pathway. Therefore, the cycle retention of Si- and Sn-based anode materials is affected by the interaction of multiple factors and to obtain good cycle retention of Si- and Sn-based anodes still require further improvements. [12].

Pb has not received much attention due to its toxic nature and volume expansion problem (233%). Nevertheless, several studies have been conducted on this topic because of its affordability [13–16]. Pb-based composite recently was proposed as an anode material with excellent reversible capacity and cycle stability, suggesting that carbon was used to suppress volume expansion through an easy synthesis of a high-energy ball milling (HEBM) process. [17, 18]. Inspired by the above-mentioned studies, we utilized Ge as an anode material. Ge, another group IV element, has not received any serious consideration as a new anode material for Li-ion batteries because of its high cost. In recent years, Ge has garnered significant interest due to its impressive characteristics, which include a high theoretical capacity of 1624 mAh g^{-1}, excellent electronic conductivity, and ionic diffusivity. Despite the relatively high cost of Ge, these attributes make Ge-based materials a promising choice for anodes in high-power LIBs [19–22].

In this study, we synthesized a Ge/GeO_2/C composite anode material (Ge@GeO_2-C composite) for practical applications via HEBM. The exceptional chemical and physical properties of Ge@GeO_2-C particles were thoroughly characterized using X-ray photoelectron spectroscopy (XPS), X-ray diffraction (XRD), scanning electron microscopy (SEM), and transmission electron microscopy (TEM) analyses. To assess its suitability as an anode material in LIBs, the electrochemical properties of Ge@GeO_2-C were evaluated using dQ/dV and galvanostatic charge–discharge procedures. Additionally, post-mortem characterization was performed to enhance our understanding of the Ge@GeO_2-C composite materials. Our findings offer compelling evidence that Ge@GeO_2-C has significant potential for advancing high-energy–density LIBs owing to its interesting material properties.

Experimental Aspects

Preparation & Characterization of Ge@GeO_2-C Anode

Ge@GeO_2-C was produced via HEBM using GeO_2 (Sigma Aldrich, 99%) and Super P carbon (Timcal, C45). A stainless-steel vial was used for the high-energy ball milling which was purchased from Cole-Parmer Inc. The stainless-steel vial with a volume size of 65 ml containing GeO_2 and Super P in a 7:3 weight ratio was assembled in an argon-filled glove box to prevent any reaction with oxygen. The high-energy ball milling (SPEX 8000 M mill grinder, Spex Sample Prep Co.) was performed for 1, 3, and 5 h. In the case of the SPEX 8000 M mill grinder, the maximum running time was 100 min, so to ensure the reliability of the experiment, the experiment was conducted for 60 min at a time, and the next turn was started immediately after 60 min. The synthesized anode materials were stored in the glove box to prevent any reactions with oxygen. Subsequently, an electrode was fabricated by applying a mixed slurry to the copper foil current collector. XRD was conducted with a Panalytical X-ray diffractometer equipped with a Cu-Kα X-ray source (λ = 1.5406 Å) and XRD pattern 2Theta starts from 10° to 80° at a scan rate of 1° min^{-1}. Sample morphologies were assessed using field-emission scanning microscopy at the Korea Basic Science Institute in Daejeon (FE-SEM, S-4800, Hitachi, Japan).

High-resolution transmission electron microscope (HRTEM) and energy-dispersive X-ray spectroscopy (EDS) images were obtained using an ultra-corrected, energy-filtered TEM microscope (Libra 200 HT MC Cs, Carl Zeiss, Germany) at an acceleration voltage of 200 kV. For sample preparation of TEM analysis, a drop of a dilute solution of nanoparticles in ethanol was coated onto ultrathin carbon-deposited copper girds.

The XPS analysis was conducted using a Thermo Fisher Scientific X-ray photoelectron spectrometer. The spectra were obtained using Al-Kα radiation (spot size: 200 µm), and the depth profile was collected via Ar ion beam etching. Prior to sputtering, a pristine surface profile was collected; then the etched profile was collected after 30 min. The XPS analysis was performed at the Converging Materials Core Facility of Dong-Eui University.

Cell Assembly and Electrochemical Testing

The mixing ratio of slurry used for the electrode comprised 73% Ge@GeO_2-C powder, 9% Super P carbon, and 18% polyvinylidene difluoride (PVDF, Solvay Olef 5130) and mixed with N-methylpyrrolidone solvent using a THINKY Mixer (ARE-310). The mixing ratio was chosen based on the previous literatures [17, 18].

The cast electrode foil was then dried in a convection oven at 90 °C for 12 h. The fabricated electrodes were roll pressed and cut into a circle (14 mm diameter) with mass density of 2.28–2.67 $mgcm^{-2}$ of active material. CR-2032 Li half-cells (Li metal/Ge@GeO_2-C electrode) were assembled in an argon-filled glove box with oxygen and moisture levels of less than 0.1 ppm as negligible amount [24]. Commercial 1 M $LiPF_6$ in EC:DEC (1:1 vol) (10 wt% FEC added) electrolytes and a Celgard® separator were used to conduct electrochemical performance tests (WonATech, WBCS3000) under a 30 °C chamber for discharge–charge cycling studies.

Results and Discussion

Synthesis and Characterization of Ge@GeO_2-C

The HEBM method involves subjecting raw materials to forceful impact, grinding, and stirring of hard balls through the rotation or vibration of the ball mill. This crushes the bulk materials into nano- and microparticles, resulting in mechanical alloying. This method has gained popularity in industry owing to its advantages over the traditional chemical route, including lower cost-effectiveness, the lack of need for precise temperature or pressure control in large-scale production processes, and the effective production of fine, uniformly dispersed particles. Figure 1 shows the Ge@GeO_2-C composite material production scheme using the simple HEBM technique. Owing to the high malleability of alloy metals (Ge, Pb, Sn, Si, etc.), size control cannot be achieved by directly milling the material. To obtain mechanically well-pulverized particles, bulk GeO_2 particles were reduced to metallic Ge by carbon-thermal reduction of GeO_2 with Super P ($2GeO_2 + 2C \rightarrow 2Ge + 2CO_2$) during HEBM. This produces Ge@GeO_2-C core–shell particles that are evenly implanted in a carbon matrix in the form of a composite. The unreacted carbon acts as a composite matrix that improves electrical connectivity and mitigates the stress caused by the significant volume expansion of active Ge during lithiation [17]. The XRD and XPS data below gives insight into the core–shell structure's origins. Figure 2a displays the Ge@GeO_2-C's XRD patterns with respect to the milling time (1, 3, and 5 h). The XRD pattern of the commercial GeO_2 used as starting material exhibited a sharp GeO_2 (101) peak. The prepared Ge@GeO_2-C patterns clearly displayed a prominent peak corresponding to the metallic Ge (111) peak as the synthesis time increased. As can be seen by comparing the (111) peaks, the peak broadening increases as ball milling progresses, which indicates that the particle size decreases. The Scherrer equation calculated the Ge@GeO_2-C (5 h) crystalline size to be approximately 4.2 nm. The wide background at approximately 25–35° was attributed to Super P. The presence of GeO_2 in the as-prepared sample can be explained in two ways. After ball milling, the surface of Ge nanoparticles may have an unreacted reside of starting GeO_2 or a self-limiting native oxide layer formed [25]. The GeO_2-shell-on-Ge-core nanoparticle structure was further confirmed by high-resolution X-ray photoelectron spectroscopy (XPS) depth-profile measurement (Fig. 2b). A prominent peak was observed in the pre-sputter data at 33 eV, which corresponds to the binding energy of Ge–O. The metallic Ge signal at 30 eV had a minimal peak strength, indicating that GeO_2 was the primary surface chemical component of the Ge@GeO_2-C particles. In contrast to that of pre-sputtering, the XPS spectra obtained

Fig. 1 Schematic illustration of high-energy ball milling for synthesis of the Ge@GeO_2-C composite material

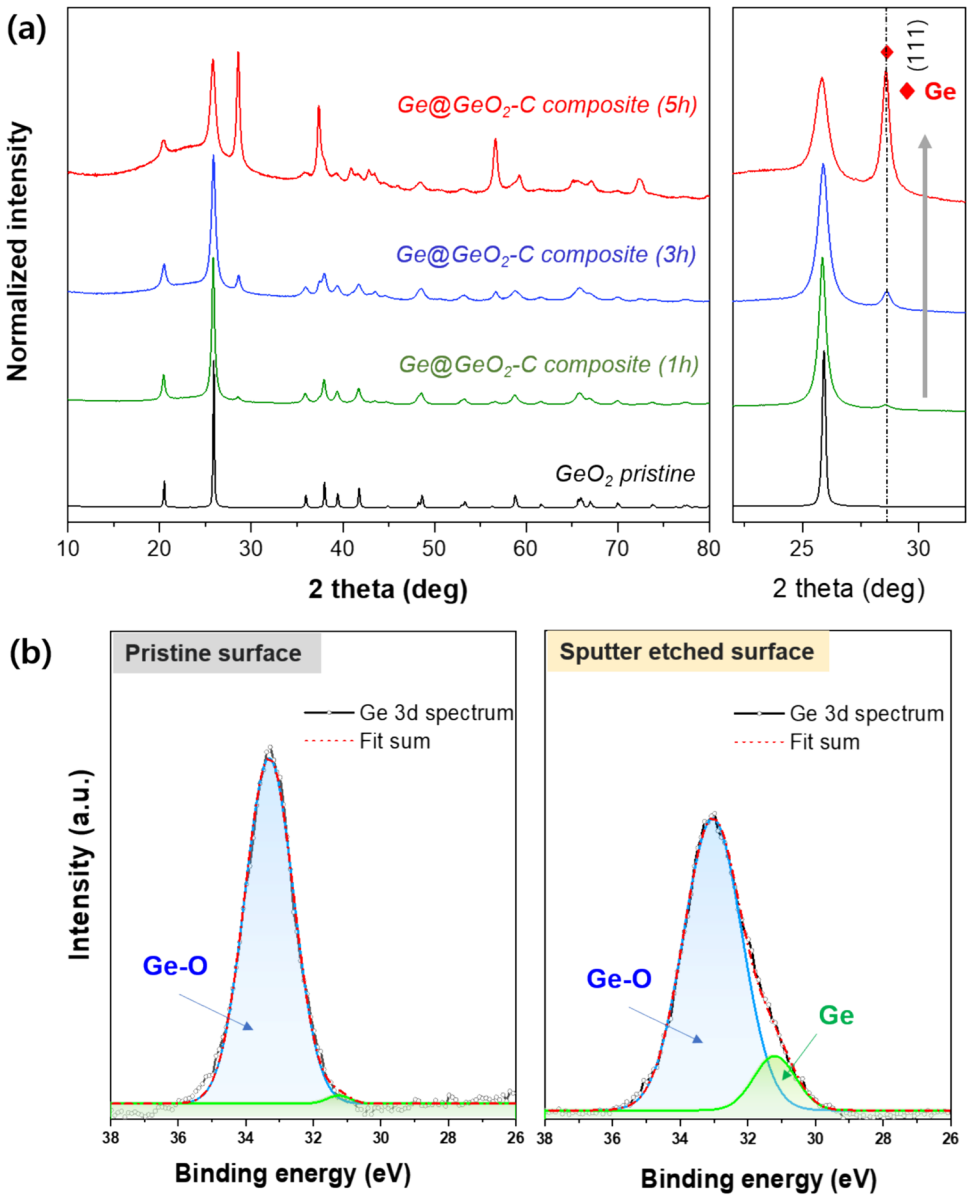

Fig. 2 **a** XRD patterns of the pristine GeO_2 and Ge@GeO_2-C composite materials based on high-energy ball milling time (1, 3, and 5 h). **b** XPS spectra of the Ge@GeO_2-C composite (5 h) material, measured on the pristine surface and sputter-etched surface

after surface sputtering exhibited a larger metallic Ge signal (30 eV) because the underlying metallic Ge core was visible owing to the etching of the GeO_2 layer. The shapes and morphologies of the prepared Ge@GeO_2-C were confirmed by field-emission SEM (Fig. 3a–c). Three SEM images are shown according to ball milling time (1 h, 3 h, 5 h). Basically, the SPEX 8000 M mill grinder is a ball-milling machine that breaks particles into small pieces within few mins, as the ball milling time increases, the particle size decreases when SEM was measured using same 5 µm scale bar. The average diameter of the Ge@GeO_2-C particles was submicron, providing a mostly spherical shape. HRTEM was performed to further elucidate the cluster morphology. Figure 3d and e show spherical Ge@GeO_2-C nanoparticles that are approximately 10 nm in size. EDS maps showed a uniform elemental distribution of Ge, O, and C throughout Ge@GeO_2-C. In particular, in Fig. 3d, the low- and high-magnification TEM images show that crystalline nanoparticles a few nanometers in size are uniformly embedded in the carbon matrix. Based on the abovementioned results, we confirmed that Ge@GeO_2-C particles can be successfully obtained with a facile synthesis compared to previous methods using HEBM.

Electrochemical Performance and Fundamental Consideration of Ge@GeO_2-C

The electrochemical properties of Ge@GeO_2-C were compared with respect to the samples (1, 3, and 5 h) by voltage profiles and differential capacity (dQ/dV), which were

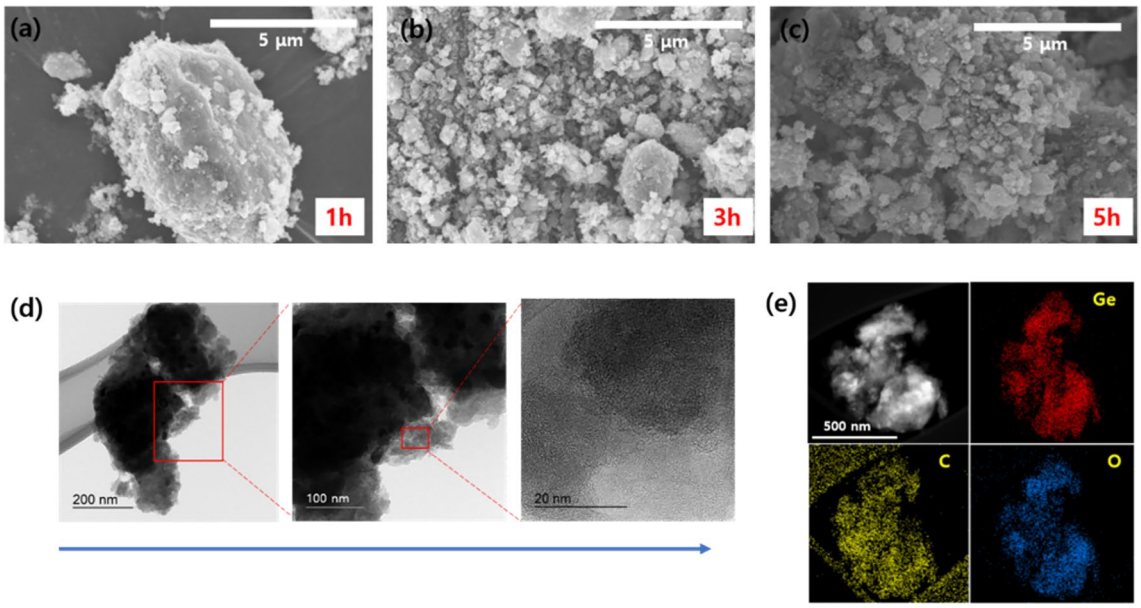

Fig. 3 **a**, **b**, **c** SEM images of Ge@GeO_2-C composite materials based on high-energy ball milling time (1, 3, and 5 h). **d** Low- and high-magnification TEM images of the Ge@GeO_2-C composite material (5 h). **e** EDS mapping of O, C, and Ge

cycled in a lithium half-cell at a current rate of 1/60 between 0.005 and 1.5 V vs Li/Li^+. In the initial cycle, the specific capacities for discharging (i.e., lithiation) and charging were 1782/528 mAh g^{-1} (1 h), 1795/780 mAh g^{-1} (3 h), and 1765/838 mAh g^{-1} (5 h) (1C = 1800 mAh g^{-1}, Fig. 4a and b). As expected, the first discharge showed high capacities, and the initial Coulombic efficiencies were 30%, 43%, and 47%m, respectively. The various voltage plateaus and dQ/dV peaks are generally linked to two electrochemical processes: (1) the displacement-conversion reaction from GeO_2 to Ge in the upper voltage region (> 1.0 V) and (2) the alloying reaction of Ge with Li in the lower voltage region (1.0 V). During the initial discharging process, the occurrence of voltage plateaus (corresponding dQ/dV peaks) at 1.2 V can be attributed to the conversion reaction of GeO_2. (1) Conversion of GeO_2 to the metallic Ge phase. The two peaks below 1.0 V (0.2 and 0.54 V) are attributed to the alloying reaction of Ge with Li in the lower-voltage region. During the reverse step, the peaks at 0.4 V are attributed to the de-alloying and oxidation of Ge. Based on the aforementioned results, the capacity difference among the three samples (1, 3, and 5 h) is attributed to the higher amount of metallic Ge (5 h > 3 h > 1 h).

$$\text{Conversion reaction } \left(> 1.0 \text{ V vs } Li/Li^+\right): \quad GeO_2 + 4Li \rightarrow 2Li_2O + Ge \tag{1}$$

$$\text{Alloying reaction } \left(< 1.0\text{V vs } Li/Li^+\right): \quad Ge + 4.25Li \leftrightarrow Li_{4.25}Ge \tag{2}$$

Figure 4c and d show the charge–discharge performance for the first cycles and dQ/dV plots cycled at a current rate of 1/30 between 0.005 and 1.5 V vs Li/Li^+. The specific capacities for discharging/charging are 1729/525 mAh g^{-1} (1 h), 1741/803 mAh g^{-1} (3 h), and 1752/811 mAh g^{-1} (5 h). The initial Coulombic efficiencies are 30%, 46%, and 46.2%, respectively. The overall trend was found to be consistent with the aforementioned description, showing no significant deviation. The formation of irreversible Li_2O during a conversion reaction causes the charging capacity to decrease as the GeO_2 ratio increases. Therefore, as the metallic Ge ratio increases, a reversible alloying reaction occurs, which increases the charge capacity.

Figure 5a illustrates the cyclic characteristics of Ge@GeO_2-C cells (1, 3, and 5 h) at a current rate of 1/30 between 0.005 and 1.5 V for 10 cycles, which show an increased discharge capacity with increased milling time, as described above. However, the cyclic performance requires improvement. To understand the capacity fading, the corresponding post-mortem SEM images were characterized (Fig. 5b) after 30 cycles. The surface SEM images show increased cracks on the surface and size at the same scale, which may have decreased the performance of the cell by isolating active particles from the Cu foil compared to the pristine sample. Despite carbon being employed to create a buffer layer in a composite, it is still not sufficient to prevent the volume expansion of 370%, as we stated in the introduction.

Based on these results, poor cycling properties were considered according to the recent literatures: (1) huge volume

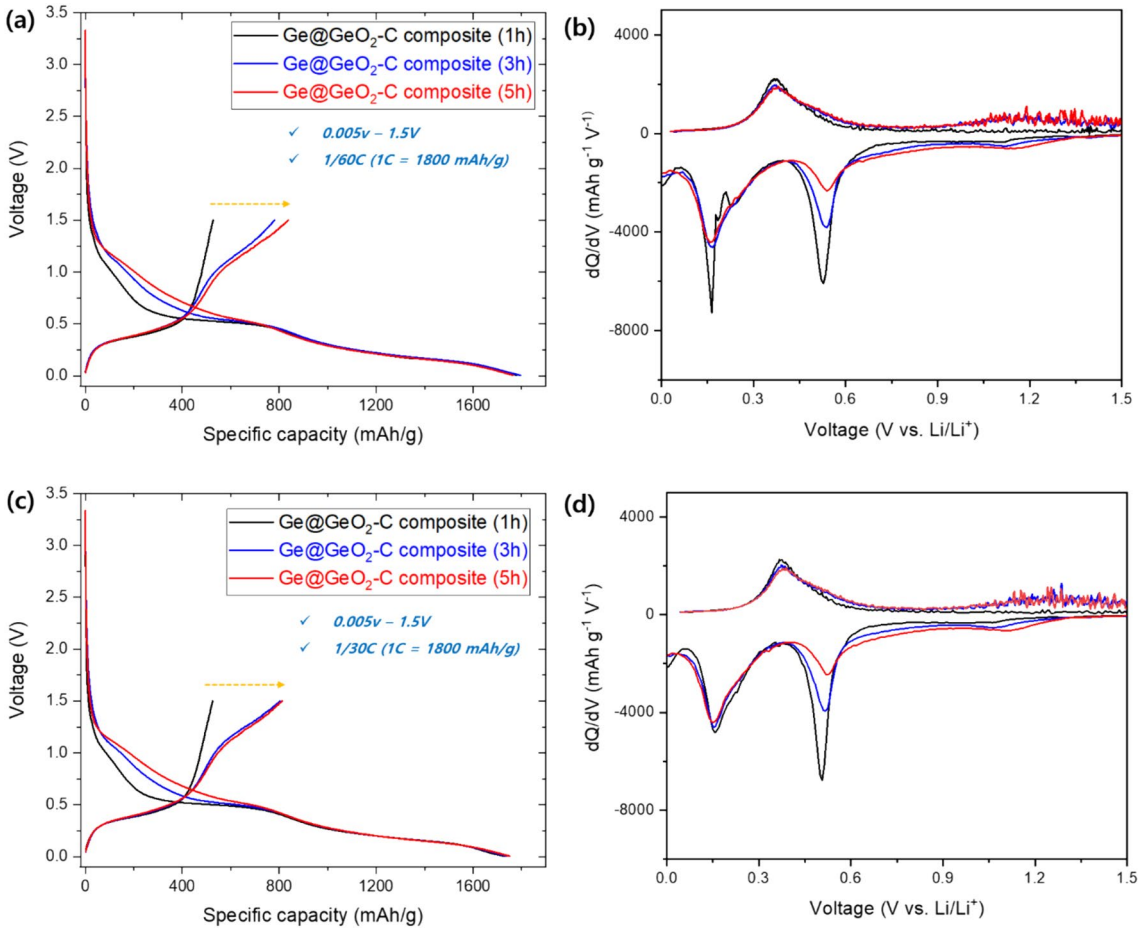

Fig. 4 **a** Initial voltage profiles and **b** differential capacity plots (dQ/dV) of Ge@GeO_2-C composite anodes cycled in a Li half-cell at a 1/60C C-rate between 0.005 V and 1.5 V versus Li. **c** Initial voltage profiles and **d** differential capacity plots (dQ/dV) of Ge@GeO_2-C composite anodes cycled at a 1/30C C-rate between 0.005 V and 1.5 V versus Li

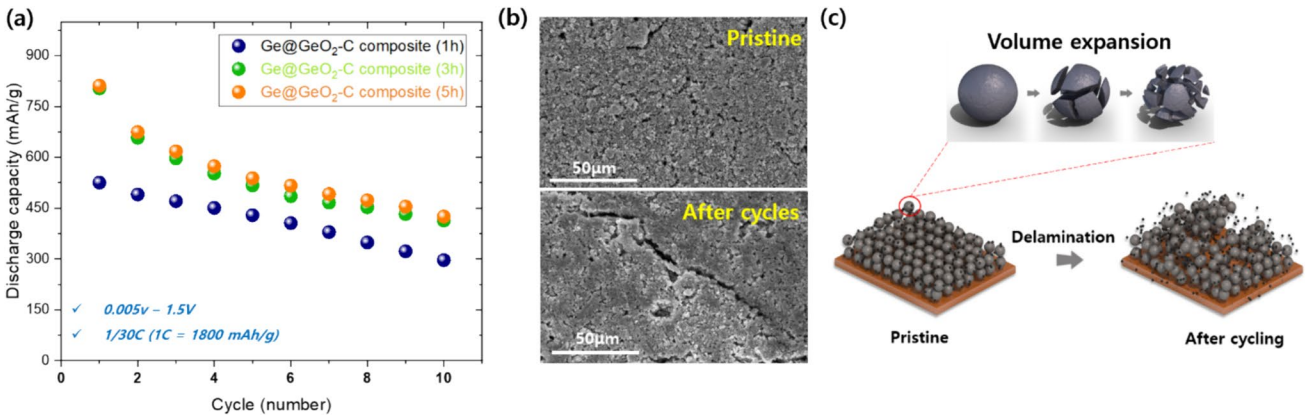

Fig. 5 **a** Discharge capacity versus cycle number for Ge@GeO_2-C composite anodes in Li half-cells at a 1/60C C-rate between 0.005 V and 1.5 V versus Li. **b** SEM images of pristine and cycled (30 cycles) Ge@GeO_2-C composite (5 h) electrodes. **c** Schematic of the proposed degradation mechanism due to volume expansion after cycling

change of Ge upon lithiation/delithiation, resulting in pulverization; and (2) delamination during the cycles leading to electrical isolation as well as SEI layer decomposition, as shown in Fig. 5c [8, 26, 27]. These results indicate that further research is required to improve the performance by considering the parameters (milling time, ratio of components, synthesis temperature, etc.). Similar to the previous study on Pb by J. Han et al., carbon was expected to act as a sufficient buffer layer during volume expansion; however, the Ge particles appear to have broken down rapidly during cycling. Further research is required to form a good SEI layer, including studies on electrolyte additives, carbon, SWCNT(Single Wall Carbon Nanotube), CNT(Carbon Nanotube), Ge mixing composition ratios, and the use of other water-based binders (CMC/SBR binder etc.). Nevertheless, three sample case studies according to ball milling time were conducted to examine the characteristics of Ge anode material through XRD, SEM, XPS and TEM methods despite no significant improvement in cycling performances. We hope that the HEBM synthesis method, which is simple and easy to mass-produce compared to previous studies, will contribute to the development of next-generation Ge anode materials.

Conclusion

GeO_2/Carbon (Ge@GeO_2-C composite) was synthesized using a simple HEBM process to address the limitations of current anodes. The GeO_2-shell-on-Ge-metal core composite was characterized using XRD, SEM, XPS and TEM analyses. As the ball milling time increased, the proportion of metallic Ge increased because of the reduction reaction, and the discharge capacity also increased. The Ge@GeO_2-C composite was evaluated for its electrochemical properties via differential capacity analysis (dQ/dV) and the galvanostatic charge–discharge technique to determine its suitability as an anode material for LIBs. The initial discharge capacity reached approximately 1800 mAh g^{-1} at a rate of C/30 (Ge@GeO_2-C composite, 5 h); however, it exhibits poor cycling retention over 10 cycles. The carbon matrix was expected to alleviate the volume expansion of Ge (370%); but, the post-mortem SEM images showed that the composite cracked and delaminated from the Cu foil after only 30 cycles. Although improvements are required, a case study was carried out on three samples according to ball milling time using XRD, SEM, XPS and TEM methods and we hope that these findings will contribute to the future development of advanced LIBs.

Acknowledgements This work was supported by the Bisa Research Grant of Keimyung University in 2023 (Project No: 20230674) and a Commercialization Promotion Agency for R&D Outcomes (COMPA) grant funded by the Korean Government (Ministry of Science and ICT) (grant number RS-2023-00304768).

Data availability The datasets used and/or analysed during the current study available from the corresponding author on reasonable request.

References

1. T. Kim, W. Song, D.-Y. Son, L.K. Ono, Y. Qi, Lithium-ion batteries: Outlook on present, future, and hybridized technologies. J. Mater. Chem. A **7**, 2942 (2019)
2. M. Li, J. Lu, Z. Chen, K. Amine, 30 years of lithium-ion batteries. Adv. Mater. **30**, 1800561 (2018)
3. A. Manthiram, An outlook on lithium ion battery technology. ACS Cent. Sci. **3**, 1063 (2017)
4. P. Li, J.-Y. Hwang, Y.-K. Sun, Nano/microstructured silicon–graphite composite anode for high-energy-density li-ion battery. ACS Nano **13**, 2624 (2019)
5. X. Zuo, J. Zhu, P. Müller-Buschbaum, Y.-J. Cheng, Silicon based lithium-ion battery anodes: a chronicle perspective review. Nano Energy **31**, 113 (2017)
6. M. Obrovac, L. Christensen, D.B. Le, J.R. Dahn, Alloy design for lithium-ion battery anodes. J. Electrochem. Soc. **154**, A849 (2007)
7. C.K. Chan, X.F. Zhang, Y. Cui, High capacity li ion battery anodes using Ge nanowires. Nano Lett. **8**, 307 (2008)
8. J.W. Choi, D. Aurbach, Promise and reality of post-lithium-ion batteries with high energy densities. Nat. Rev. Mater. **1**, 1 (2016)
9. C. Zhang, F. Wang, J. Han, S. Bai, J. Tan, J. Liu, F. Li, Challenges and recent progress on silicon-based anode materials for next-generation lithium-ion batteries. Small Str. **2**, 2100009 (2021)
10. Y. Jin, B. Zhu, Z. Lu, N. Liu, J. Zhu, Challenges and recent progress in the development of Si anodes for lithium-ion battery. Adv. Energy Mater. **7**, 1700715 (2017)
11. J.-H. Cho, S.T. Picraux, Silicon nanowire degradation and stabilization during lithium cycling by SEI layer formation. Nano Lett. **14**, 3088 (2014)
12. K. Feng, M. Li, W. Liu, A.G. Kashkooli, X. Xiao, M. Cai, Z. Chen, Silicon-based anodes for lithium-ion batteries: from fundamentals to practical applications. Small **14**, 1702737 (2018)
13. A. Dey, Electrochemical alloying of lithium in organic electrolytes. J. Electrochem. Soc. **118**, 1547 (1971)
14. F. Lipparoni, F. Bonino, S. Panero, B. Scrosati, Electrochemical properties of metal oxides as anode materials for lithium ion batteries. Ionics **8**, 177 (2002)
15. M. Martos, J. Morales, L. Sanchez, Lead-based systems as suitable anode materials for Li-ion batteries. Electrochim. Acta **48**, 615 (2003)
16. L. Peraldo Bicelli, B. Rivolta, F. Bonino, S. Maffi, C. Malitesta, Lead oxides as cathode materials for voltage-compatible lithium cells. J. Power Sour. **18**, 63–74 (1986)
17. J. Han, J. Park, S.M. Bak, S.B. Son, J. Gim, C. Villa, X. Hu, V.P. Dravid, C.C. Su, Y. Kim, New high-performance Pb-based nanocomposite anode enabled by wide-range Pb redox and Zintl phase transition. Adv. Func. Mater. **31**, 2005362 (2021)
18. J. Park, J. Han, J. Gim, J. Garcia, H. Iddir, S. Ahmed, G.-L. Xu, K. Amine, C. Johnson, Y. Jung, Evidence of Zintl intermediate phase and its impacts on li and na storage performance of Pb-based alloying anodes. Chem. Mater. **35**, 4171–4180 (2023)
19. L.C. Loaiza, L. Monconduit, V. Seznec, Si and Ge-based anode materials for Li-, Na-, and K-ion batteries: a perspective from structure to electrochemical mechanism. Small **16**, 1905260 (2020)

20. K.H. Seng, M.H. Park, Z.P. Guo, H.K. Liu, J. Cho, Self-assembled germanium/carbon nanostructures as high-power anode material for the lithium-ion battery. Angew. Chem. **124**, 5755 (2012)
21. S. Yoon, C.-M. Park, H.-J. Sohn, Electrochemical characterizations of germanium and carbon-coated germanium composite anode for lithium-ion batteries. Electrochem. Solid-State Lett. **11**, A42 (2008)
22. A.M. Chockla, K.C. Klavetter, C.B. Mullins, B.A. Korgel, Solution-grown germanium nanowire anodes for lithium-ion batteries. ACS Appl. Mater. Interfaces **4**, 4658 (2012)
23. X. Liu, X.-Y. Wu, B. Chang, K.-X. Wang, Recent progress on germanium-based anodes for lithium ion batteries: Efficient lithiation strategies and mechanisms. Energy Storage Mater. **30**, 146 (2020)
24. X. Han, S. Xia, J. Cao, C. Wang, M. Chen, Effect of humidity on properties of lithium-ion batteries. Electrochem. Sci. **16**, 210554 (2021)
25. C. Leygraf, I. O. Wallinder, J. Tidblad, T. Graedel, Atmospheric corrosion, John Wiley & Sons (2016)
26. S. Chae, S.H. Choi, N. Kim, J. Sung, J. Cho, Integration of graphite and silicon anodes for the commercialization of high-energy lithium-ion batteries. Angew. Chem. Int. Ed. **59**, 110 (2020)
27. Y. Jin, S. Li, A. Kushima, X. Zheng, Y. Sun, J. Xie, J. Sun, W. Xue, G. Zhou, J. Wu, Self-healing sei enables full-cell cycling of a silicon-majority anode with a coulombic efficiency exceeding 99.9%. Energy Environ. Sci. **10**, 580 (2017)